Resonant photodetector for cavity- and phase-locking of squeezed state generation

Chaoyong Chen, Zhixiu Li, Xiaoli Jin, and Yaohui Zheng

Citation: Rev. Sci. Instrum. **87**, 103114 (2016); doi: 10.1063/1.4966249
View online: http://dx.doi.org/10.1063/1.4966249
View Table of Contents: http://aip.scitation.org/toc/rsi/87/10
Published by the American Institute of Physics

Resonant photodetector for cavity- and phase-locking of squeezed state generation

Chaoyong Chen, Zhixiu Li, Xiaoli Jin, and Yaohui Zheng[a)]
State Key Laboratory of Quantum Optics and Quantum Optics Devices, Institute of Opto-Electronics, Shanxi University, Taiyuan 030006, China and Collaborative Innovation Center of Extreme Optics, Shanxi University, Taiyuan, Shanxi 030006, People's Republic of China

(Received 8 June 2016; accepted 14 October 2016; published online 31 October 2016)

Based on the requirement of squeezed state generation, we build the phase relationship between two electronic local oscillators for the cavity- and phase-locking branches, and a 2-way 90° power splitter is adopted to satisfy the phase relationship simultaneously, which greatly simplifies the experimental setup and adjusting process. A LC parallel resonant circuit, which is composed by the inherent capacitance of a photodiode and an extra inductor, is adopted in the resonant photodetector to improve the gain factor at the expected frequency. The gain of the resonant photodetector is about 30 dB higher than that of the broadband photodetector at the resonant frequency. The peak-to-peak value of the error signal for cavity-locking (phase-locking) with the resonant photodetector is 240 (260) times of that with the broadband photodetector, which can improve the locking performance on the premise of not affecting the squeezing degree. *Published by AIP Publishing.* [http://dx.doi.org/10.1063/1.4966249]

I. INTRODUCTION

The photodetector is widely used in diverse quantum optics experiments for different purposes.[1] Two key applications are: readout of optical squeezed state noise, which requires a low-noise, large-dynamic-range, high common-mode rejection ratio photodetector; high-frequency signal readout for cavity- and phase-locking based on the Pound-Drever-Hall (PDH) technique.[2–5] In our former works, a high-performance photodetector has been obtained for the readout of squeezed state noise based on the bootstrapped structure and differential fine tuning circuit.[6–8] For a PDH locking system, the signal coupled into the photodetector is narrow-band one at the modulation frequency, conventionally a broad bandwidth photodetector magnifies the signal and noise in the whole band, which is detrimental to improve the signal to noise ratio. As a result, the performance of squeezed state system is dropped.

In order to improve the locking performance, increasing the optical power of injected photodetector is a simple method. However, the increase of injected power is adverse to the quantum noise reduction, due to the increase of classical noise with the increase of injected power.[9] In addition, for the sake of the quantum noise reduction, we have to increase the escape efficiency of optical parametric amplifier (OPA), which deteriorates the impedance matching of OPA. The impedance mismatching does further reduce the effective power (*ac* component) of injected photodetector for cavity- and phase-locking and increase the *dc* component of detected signal. Therefore, it is inappropriate to increase the optical power for improving the locking performance in quantum optics experiments, which can be only achieved by boosting the photodetector gain.

For a simplest squeezed state generation system, there include the locking loops of the OPA cavity length and the relative phase between the pump and seed beams. These locking loops need independent photodetectors to read error signal, which add system complexity.[9] So the study focuses on the following two aspects. First, how to realize the high gain photodetection at the modulation frequency. Second, how to lock the OPA cavity length and relative phase between the pump and seed beams simultaneously.

Driven by the requirement of quantum optics experiments, a high-gain, multi-function photodetector is designed based on the parallel resonant and 2-way 90° power splitter circuits. At the modulation frequency, the gain of resonant photodetector (RPD) is about 30 dB higher than that of the broadband photodetector (BPD). The amplitudes of the PDH error signals of RPD for cavity- and phase-locking are both more 240 times than that of BPD. Moreover, we can obtain simultaneously the demodulation signal (error signal) of OPA cavity length and relative phase by using one photodetector, which greatly simplifies the experimental setup and adjusting the process of the squeezed state generation.

II. THEORY

A. Error signals generation of locking the cavity length and relative phase

Figure 1 shows the experimental setup for a squeezed state generation. Squeezed states are generated by an OPA locked on resonance. The relative phase between the pump and seed beams is locked at the de-amplified (π)/amplified (0) phase to obtain the quadrature-amplitude/phase squeezed light. A seed beam is coupled into the cavity through the high-reflective mirror. The back reflected light is separated from the incoming light by an optical isolator and is detected by two photodetectors. The OPA cavity length and relative phase between the pump and seed beams are locked using two error signals generated by demodulating the two photodetectors' outputs,

a)Electronic mail: yhzheng@sxu.edu.cn

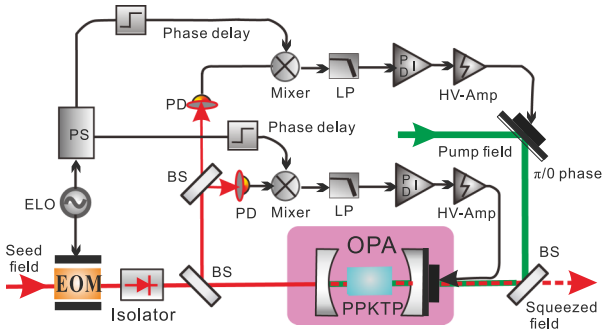

FIG. 1. A simple schematic of squeezed state generation experimental setup. A 1064 nm squeezed state is generated from a OPA which is pumped by a second harmonic 532 nm light generated in a Nd:YVO_4 solid laser. The seed beam is phase modulated at a fixed frequency, typically tens of MHz, using an electro-optical modulator (EOM). The error signals for the cavity length control and phase control can be generated separately after proper demodulation the EOM-modulation frequency via the PDH technique. PS: power splitter. PD: photodetector. BS: beam splitter. LP: low-pass filter.

respectively. The phase of the electronic local oscillator (ELO) is controlled independently to optimize the PDH error signals for cavity- and phase-locking.

For simplifying the experimental system, we analyze the phase relationship of the ELOs between cavity- and phase-locking. In the PDH setup, the reflected beams include a carrier and two sidebands. What we measure with the photodetector is the power in the reflected beam, which can be expressed as below[2]

$$P_{ref} = (dc\ terms) + 2\sqrt{P_c P_s}\{Re[\Lambda]\times\cos\Omega t + Im[\Lambda]\times\sin\Omega t\} + (2\Omega\ terms). \quad (1)$$

Here

$$\Lambda = F(\omega)F^*(\omega+\Omega) - F^*(\omega)F(\omega-\Omega). \quad (2)$$

The P_c is the power in the carrier and the P_s is the power in each first-order sideband. ω: the optical frequency. $F(\omega)$: the reflection coefficient. Ω: the modulation frequency.

The terms Ω arise from the interference between the carrier and the sidebands, and the 2Ω terms come from the sidebands interfering with each other. We are interested in the two terms that are oscillating at the modulation frequency. So a smooth gain within a broadband of the photodetector is not needed and it is enough to keep a high gain at the modulation frequency. Resonant circuit, which can amplify resonantly the photocurrent nearby the resonant frequency at the expense of narrowing the gain bandwidth,[10] meets the requirements for PDH technique very well.

When the modulation frequency Ω is far less than the linewidth of the OPA, the detected signal is purely real near resonance, and only the cosine term is important. The detected signal and ELO with the same frequency are fed into a mixer and the mixer's output forms the product of two inputs. The product of two sine waves is

$$\cos(\Omega t)\cos(\Omega t) = \frac{1}{2}\{\cos[(\Omega-\Omega)t] + \cos[(\Omega+\Omega)t]\}. \quad (3)$$

The $\cos[(\Omega+\Omega)t]$ term is isolated with a low-pass filter, the term $\cos[(\Omega-\Omega)t]$ is a *dc* signal, that is, PDH error signal.

However, if we mix a sine and a cosine signal, we get

$$\cos(\Omega t)\sin(\Omega t) = \frac{1}{2}\{\sin[(\Omega+\Omega)t] - \sin[(\Omega-\Omega)t]\}. \quad (4)$$

In this case, the *dc* signal vanishes, we cannot get the PDH error signal. As a result, if we want to obtain the PDH error signal for cavity-locking, the ELO should be a cosine signal.

The analysis above is based on the assumption that the modulation frequency is far less than the linewidth of the OPA. But when none of these conditions is present, the detected signal is not pure real but complex number. When the modulation frequency is less than the linewidth of the OPA, the cosine term is dominating. The terms Ω in expression (1) can be transferred below

$$2\sqrt{P_c P_s}\sqrt{(Re[\Lambda])^2 + (Im[\Lambda])^2}\times\cos(\Omega t+\varphi). \quad (5)$$

The phase of the detected signal φ is dependent of the relationship between the modulation frequency and linewidth. If we use a cosine signal with a fixed phase as the ELO to demodulate the detected signal, the error signal can be expressed as

$$\varepsilon = 2\sqrt{P_c P_s}\sqrt{(Re[\Lambda])^2 + (Im[\Lambda])^2}\times\cos\varphi. \quad (6)$$

For the general case of an OPA cavity, the reflection coefficient F(ω) is given by

$$F(\omega) = \frac{-r_1 + r_2(r_1^2+t_1^2)\exp(i\frac{\omega}{\Delta\nu})}{1 - r_1 r_2\exp(i\frac{\omega}{\Delta\nu})}. \quad (7)$$

Here, r_1 and t_1 are the amplitude reflection and transmission coefficients of the input mirror, r_2 is the amplitude reflection coefficient of the output mirror, and $\Delta\nu$ is the free spectral range. For a typical OPA cavity, it has these parameters: r_1 = 0.999, r_2 = 0.88, and the linewidth $\delta\upsilon$ = 50 MHz. Taking these parameters into expression (6) and expression (7), we obtain a figure of the ratio between the actual and optimal value of the error signal (the black solid line) and the phase φ of the detected signal (the red dashed line) versus the ratio between the modulation frequency and cavity linewidth (see Figure 2).

When the modulation frequency changes from 0 to the linewidth of the OPA, the φ changes from 0° to 26.5°. If the phase of demodulation signal keeps constant, we cannot obtain

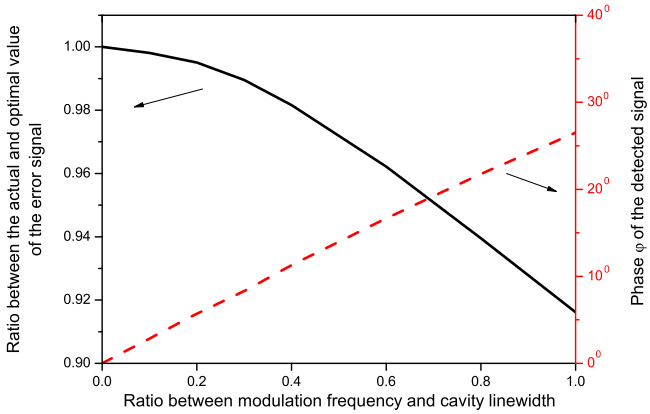

FIG. 2. The ratio between the actual and optimal value of the error signal (the black solid line) and the phase φ of the detected signal (the red dashed line) versus the ratio between the modulation frequency and cavity linewidth.

the optimal amplitude of the error signal. At the modulation frequency of 50 MHz (linewidth of the OPA), the amplitude deviation between the actual and optimal value of the error signal is maximal, the actual value is approximately 91.6% of the optimal value, the influence can be neglected. For other modulation frequency below the linewidth, the influence of the amplitude deviation becomes smaller. In addition, the zero position remains unchanged with the variation of the modulation frequency.

For the relative phase locking, the photodetector reads the interference between the modulated seed beam and pump beam, and then this signal is demodulated by ELO. According to the principle of phase-locking, the power signal detected by the photodetector can be expressed as below

$$P_{pha} = (dc\ terms) + 2\sqrt{P_c P_s}\sin\Omega t \sin\theta. \tag{8}$$

Where θ is the relative phase between the seed and pump beams. The error signal for the phase-locking is the products of the detected signal and ELO. If the ELO is a cosine signal, the *dc* signal vanishes according to the expression (4). If the ELO is a sine signal, the error signal for the phase-locking E is maximum, which can be expressed by

$$\begin{aligned} E &= 2\sqrt{P_c P_s}\sin\theta \sin\Omega t \sin\Omega t \\ &= \sqrt{P_c P_s}\sin\theta[\cos(\Omega-\Omega)t + \cos(\Omega+\Omega)t]. \end{aligned} \tag{9}$$

Therefore, if we want to get the PDH error signal for the phase-locking, the ELO should be a sine signal. From the above analysis, although the optimal demodulation phase difference, originating from the phase change of the detected signal with the modulation frequency, deviates from 90°, its influence of the phase difference on the amplitude of the error signal can be neglected. The two ELOs should be 90° out of phase to meet the requirements for locking the OPA cavity length and relative phase simultaneously.

In general, the OPA is locking on the resonance, where the reflected carriers interfere destructively, and the modulation frequency is about tens of MHz. So at this time, most noise sources fall off but only shot noise plays a very crucial role to limit the best locking performance. On resonance, the average power falling on the photodiode is approximately $2P_s$, the shot noise level in this case is then calculated to be

$$\begin{aligned} &LSD_{Upd}(f) \\ &= 20\log_{10}\left(\sqrt{(2\eta_{qe}(2P_s\frac{2\pi e^2}{h\omega})}\cdot g\cdot\frac{1}{1[V]}\right)[\frac{dBV}{\sqrt{Hz}}]. \end{aligned} \tag{10}$$

Here we mark the quantum efficiency of the photodiode as η_{qe} and the transimpedance gain factor of the detector as g.

B. LC parallel resonant circuit

Figure 3(a) shows a conventional layout of a photodetector circuit consisting of a photodiode D1, a load resistor R1, and an operational amplifier OP1. And its equivalent circuit is displayed in Figure 3(b). Rd is the dark resistance of the photodiode with a large resistance value about a few hundred megaohms, which is often neglected in the parallel circuit. Under the circumstances, a photodiode can be regarded as a current source. Photocurrent *Is* generated in the photodiode is converted into voltage by the load resistor R1 and then this voltage is amplified by the OP1. Although the resistance's increase of load resistor R1 can increase the converted voltage, which is the benefit to improve the photodetector's gain, it will bring in severe thermal noise, really low sensitivity, small dynamics range, and further cause reverse voltage fluctuations of the photodiode.[11,14] What is worse, in the conventional layout, the capacitances, including the inherent capacitance Cd of the photodiode and the parasitic capacitance associated with component interconnections, reduce the signal voltage, which limits severely its application in the high frequency detection.

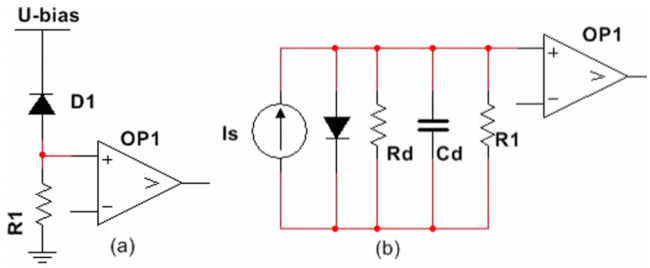

FIG. 3. Conventional layout of a photoelectric detection circuit (a) and its equivalent circuit (b). An equivalent circuit of a photodiode D1 consists of a current source, an ideal diode, an inherent capacitance Cd, and a dark resistance Rd.

In order to solve these problems above, we replace the conventional circuit with a LC resonant circuit. The advantage of the resonant circuit has been analyzed in detail in Ref. 11. Both the series resonant circuit and parallel resonant circuit can be used to process the photocurrent. However, in the series resonant circuit, the *dc* photocurrent is usually much larger than the *ac* component, which causes easily the operational amplifier saturation and is adverse to the *ac* component amplification. There needs some special design to circumvent them. In addition, in the series resonant circuit, a small inductor must be bonded in between the photodiode and the OP1, which make them difficult to fabricate.[12]

So we choose a LC resonant circuit as shown in Figure 4(a), which is composed of the inherent capacity Cd of the photodiode D1 and an extra inductor L. And its equivalent circuit is shown in Figure 4(b), which can be regarded as a parallel resonant LC circuit.[12] The parallel resonant LC circuit can serve as a current to voltage converter and convert the photocurrent generated in the photodiode into a voltage signal.[4,11] It is worth noting that the LC resonant circuit does also act as a band-pass amplifier,[11,14] which can boost the signal at the expected frequency, and suppress other signals

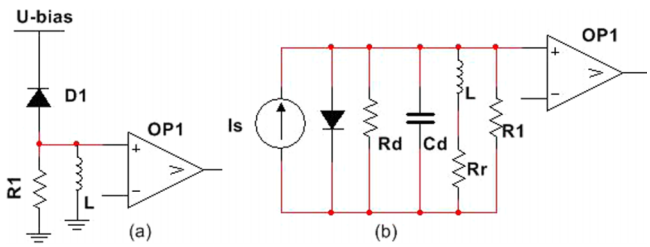

FIG. 4. Circuit layout of a photoelectric detection circuit based on the LC resonant circuit (a) and its equivalent circuit (b). Rr is the real resistor of inductor L.

at the unwanted frequency (especially low-frequency noise). The admittance of this circuit is

$$Y = \frac{Is}{V} = \frac{1}{Rd} + j\omega Cd + \frac{1}{Rr + j\omega L}. \tag{11}$$

Resonance occurs when the imaginary part of Y is zero. The resonant frequency is expressed as

$$f = \frac{\omega}{2\pi} = \frac{1}{2\pi}\sqrt{\frac{1}{LCd} - \frac{Rr^2}{L^2}}. \tag{12}$$

In general, the resistor Rr of inductor is very small, which can be omitted. The resonant frequency can be simplified as

$$f = \frac{1}{\sqrt{2\pi LCd}}. \tag{13}$$

The photocurrent can be resonantly boosted by the LC circuit nearby the resonant frequency.[13] The quality factor Q, which is related to the gain and bandwidth of the resonant circuit, is given by the following formula:

$$Q = \frac{f}{BW_{3dB}}. \tag{14}$$

Here this resonant circuit is used to transfer energy to the load and the energy consumed in the resonant circuit is negligible, so the actual impedance of the entire circuit is equal to the load impedance R1. In this case, the quality factor Q can be expressed as another form

$$Q = \frac{R1}{X}. \tag{15}$$

X is used to represent the inductive or capacitive reactance.

III. PHOTODETECTOR DESIGN

According to the principle analysis above, aiming at the application of squeezed state generation, a detailed schematic of the photodetector is given in Figure 5. The schematic includes mainly two parts: one is signal detection and amplification (left), and the other is phase shift of the ELO (right). The resonant LC circuit is surrounded by a red frame. The ETX500T, a large-area InGaAs photodiode, with high responsivity in the 800-1700 nm spectrum, is an appropriate candidate for the cavity-and phase-locking of a squeezed state generation at near-infrared spectrum.[15,16] In this configuration, the modulated photocurrent signal is picked up and resonantly amplified by the LC circuit.[14] The inductor L has three functions: an integral part of the LC resonant circuit, a *dc* (direct current) signal shunt, and a low-frequency electronic noise attenuator.[4] Careful selection of the inductor L and capacitor C5 is significant to separate *dc* and *ac* (alternating current) signals because the *ac* component is far less than the *dc* component. The photodiode D1 is supplied with an adjustable reverse bias voltage in order to change the junction capacity and adjust finely the resonant frequency.

The current feedback amplifier (CFA), with a high slew rate, is an emerging operational amplifier. It is not limited by a constant gain-bandwidth product and is very suitable for high frequency applications.[17,18] Here, we adopt the THS3201, a superior operational amplifier with unity gain bandwidth 1.8 GHz and high slew rate 10500 V/μs, as the *ac* preamplifier,[19] which meets the requirements for our experiment very well. The photocurrent generated in the photodiode D1 produces a voltage across the current to voltage converter (consists of the LC circuit and R1) and this voltage is amplified by an operational amplifier THS3201. Because the performance of CFAs is highly dependent on the feedback resistor, the feedback resistor R3 is chosen on the basis of the reference value given in the datasheet of THS3201. R7 is used to optimize the impedance match between the 50 Ω coaxial lines and the mixers. A transimpedance amplifier N2 (AD811) converts the *dc* component current to a voltage output for monitoring the laser intensity.

The detected signal (N1 output) and ELO are fed into the mixer (TUF-3), its output is the product of the two signals, error signal. The relative phase between the detected signal and

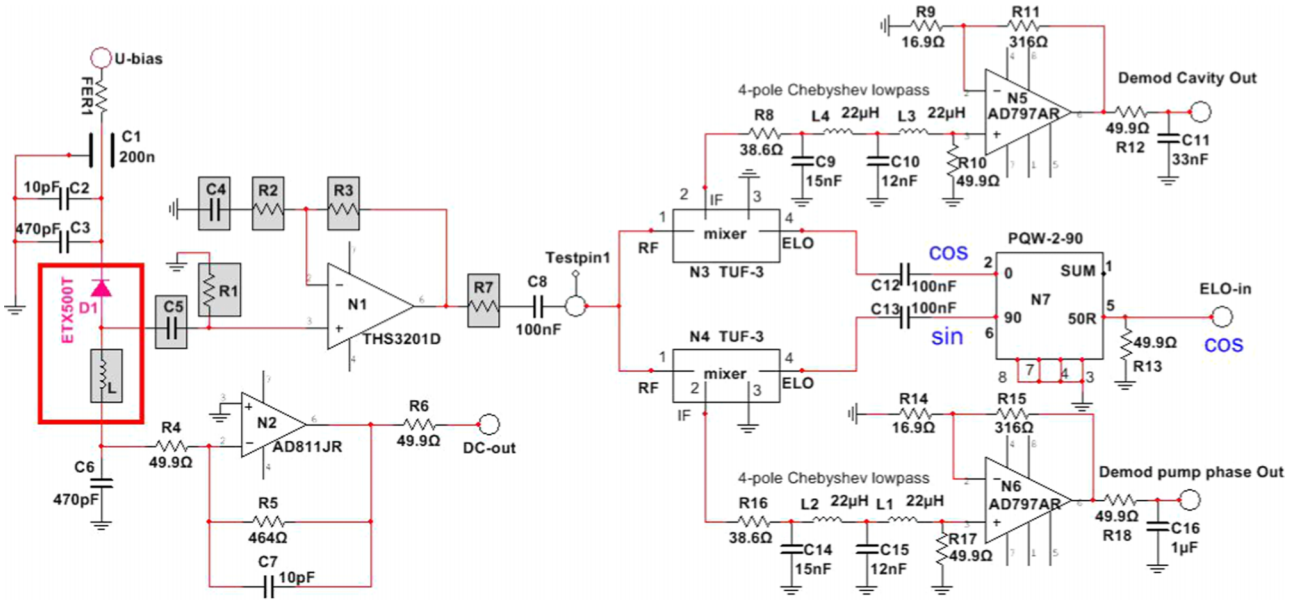

FIG. 5. Circuit schematic of the RPD. Photodiode D1 and inductor L constitute the resonant circuit. Parts with undefined values are covered by the shadow. C1 is a feed-through capacitor.

ELO is the key to optimize the error signal, which is controlled by adjusting independently the ELO phase of each branch (cavity- and phase-locking). According to the analysis of Section II, we know the desired phase for the cavity- and phase-locking branches is not mutually independent but has inherent relationship. There should be 90° out of phase between two ELOs. The ELO signal goes into a two-way 90° power splitter circuit PQW-2-90, where the split signals have 90° out of phase, which meets the requirement for the cavity- and phase-locking branches. The two split signals go into mixers (N3 and N4) to obtain the demodulated signal.

A 4-pole Chebyshev low-pass filter composed by two inductors L3, L4 and two capacitors C9, C10 is used to extract the low-frequency error signal for cavity-locking from the demodulated signal. The error signal is enlarged by N5, an operational amplifier AD797. The AD797 is a low noise, low distortion operational amplifier which is ideal for the amplification of low-frequency signal.[20] The phase-locking branch has same circuit structure as the cavity-locking branch. With the aid of a two-way 90° power splitter, we simplify the adjusting process of the relative phases between the detected signal and ELOs for cavity- and phase-locking from two independent steps to one.

In addition, as we know the error signal is a low frequency signal, typically below tens of kHz, which is susceptible to all of the low-frequency noises, such as power supply noise, amplifier noise, thermal noise, shot noise, and 1/f noise. What is more, the *ac* component of the detected signal is very weak, which is easily overwhelmed by these noises described above. So some special design is adopted to suppress the low-frequency noise. On account of the frequencies both the detection signal and the ELO are consistent with the modulation frequency, typically tens of MHz, it is an effective way of inserting high-pass filters in the circuit before mixers. In view of this, two high-pass filters, composed by C5 and R1, C4 and R2, are inserted into the circuit to suppress the low frequency noise. At the same time, lots of voltage regulator tubes and filter capacitors are used in the power supply circuit (not shown in Figure 5) to isolate the power supply noise.

A proper layout of a printed circuit board (PCB) is a very important task to realize efficiently the performance of the circuit, especially, in the high-frequency signal applications. For instance, all tracks around the THS3201 should be kept as short as possible, and the circuit should be built carefully to limit the noise coupling and parasitic capacitance. In addition, impedance matching considerations should also be taken into account in the high frequency circuit.[13,19]

IV. EXPERIMENTAL AND RESULTS

A. Transfer function

In the PDH technique, the frequency of the detected signal depends on the modulation frequency, and the resonant frequency of RPD should be tuned to make the gain maximum at the modulation frequency. The photodetector gain can be characterized by a transfer function in the frequency domain. Figure 6 shows the block diagram of measuring the transfer function of a photodetector. A laser beam with the intensity

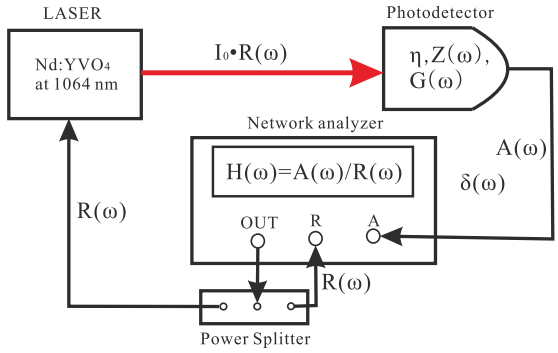

FIG. 6. Block diagram for the measurement of the transfer function.

of I_0 is modulated by an internal reference signal $R(\omega)$ from a network analyzer (Agilent 4395A). The modulation frequency can be continuously tuned at the predefined range. This amplitude modulated laser beam is sensed by a photodetector and then fed into the network analyzer $A(\omega)$. The network analyzer performs a normalized measurement by calculating the ratio $H(\omega)$ between the photodetector output $A(\omega)$ and internal reference signal $R(\omega)$. The process can be expressed by

$$H(\omega) = \frac{A(\omega)}{R(\omega)} = \frac{I_0 \cdot R(\omega) \cdot \eta \cdot Z(\omega) \cdot G(\omega) \cdot \delta(\omega)}{R(\omega)}. \quad (16)$$

Where, η is the responsivity of the photodiode ETX500T. $Z(\omega)$ is the total impedance of the current to voltage converter and its value changes with frequency. $G(\omega)$ and $\delta(\omega)$ are the total gain and total loss, respectively. According to the principle described above, we measure the transfer function of the RPD and BPD under the same conditions, respectively (shown in Figure 7). At the resonant frequency (58.6 MHz), RPD's amplitude is about 30 dB higher than that of BPD. The result shows that the resonant design can increase effectively the gain factor of the photodetector at the desired frequency, which can improve the stability of a squeezed state system without any quantum noise reduction. The 3 dB bandwidth of RPD is 0.6 MHz. The quality factor Q of the RPD can be

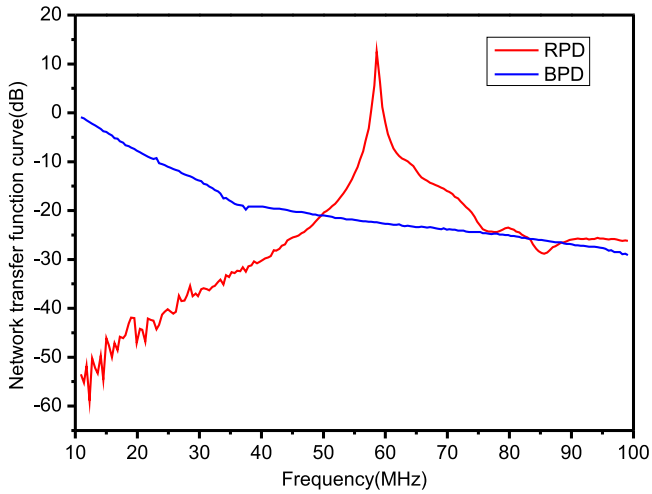

FIG. 7. The transfer functions of RPD and BPD. The resonant frequency is 58.6 MHz and the 3 dB bandwidth of RPD is 0.6 MHz. The values of the electronic components which are covered by the shadow are given (C5 = 6 pF, R1 = 20 KΩ, R3 = 464 Ω, R2 = 51.1 Ω, C4 = 33 pF, R7 = 47 Ω.).

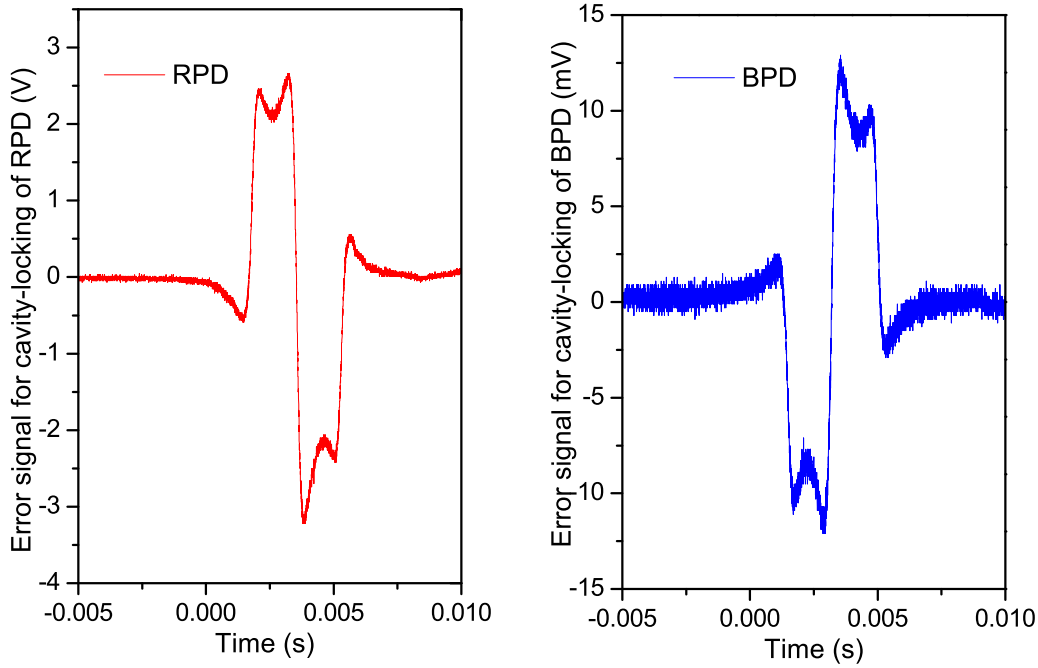

FIG. 8. Comparison of the error signals for cavity-locking of BPD (blue) and RPD (red).

calculated from the measured result by the formula (14),

$$Q = \frac{f}{BW_{3dB}} = \frac{58.6MHz}{0.6MHz} = 97.6. \quad (17)$$

The quality factor Q is also estimated by the load resistor R1 (20 kΩ) and inductor L (600 nH),

$$Q = \frac{R1}{\omega L} = \frac{20k\Omega}{2\pi \times 58.6MHz \times 600nH} = 90.6. \quad (18)$$

The quality factors from two formulas are nearly equal, which show the energy consumed in the resonant circuit is negligible.

Resonant frequency depends on the inherent capacity Cd and an extra inductor L, which can be tuned conveniently by changing the value of the inductor L and the reverse voltage of the photodiode D1 according to the formula (13) on the basis of the actual modulation frequency. However, the narrow resonance peak of the RPD will limit the bandwidth of the locking system to some degree, which should be considered in an actual locking system.

B. Error signals

According to the feedback control theory, the slope (amplitude) of the error signal near the stable point determines the sensitivity and stability of the control system.[21,22] In order to confirm that the RPD can improve the performance of

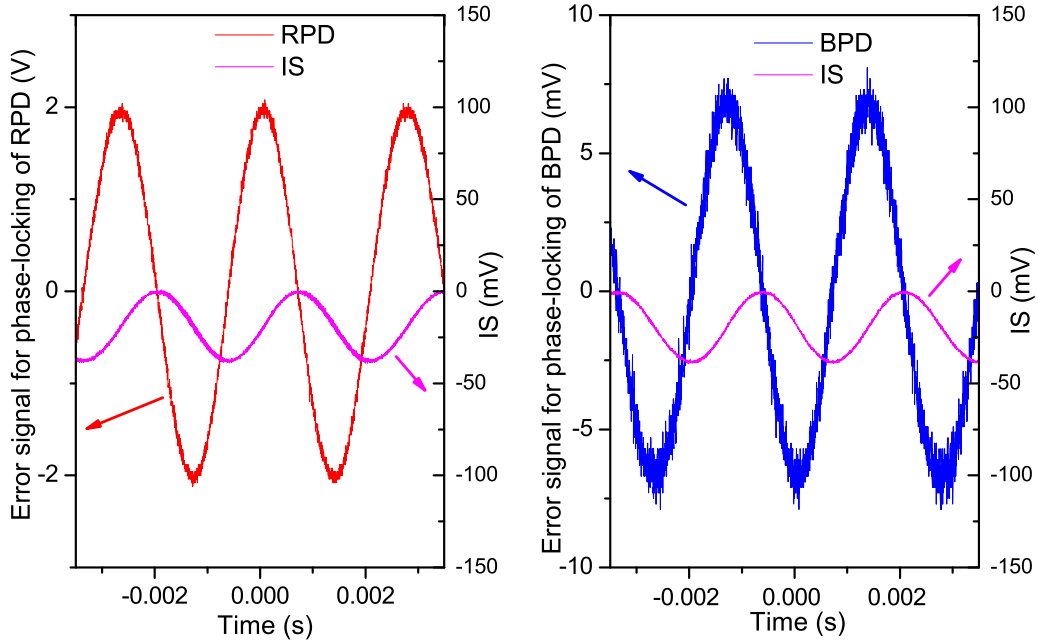

FIG. 9. Comparison of the error signals for phase-locking of BPD (blue) and RPD (red). The magenta curve is the interference signal (IS).

cavity- and phase-locking, we further compare the amplitude of the error signal by using RPD and BPD under the same conditions, respectively. For the OPA with a coupling factor of 0.05, when the seed power equals to 1 mW, the *ac* component of the injected photodetector is only 50 μW. When the modulation depth is 0.1, the peak-to-peak value of the error signal is only 25 mV, where the BPD is used. While the peak-to-peak value of the error signal is about 6 V with the RPD (Figure 8), which is 240 times with the BPD. In other words, with only 1/240 of the seed power with the BPD, we can obtain the same locking performance with the RPD, which is the benefit of reducing the classical noise of squeezed state generation.

In addition, the error signals for phase-locking are also compared, which is shown in Figure 9. When the BPD is used, the peak-to-peak value of the error signal is only 16 mV, which is only 1/260 of that with the RPD. It is worth noting that the RPD integrates the high-pass filters to suppress the low-frequency noise, the LC band-pass filter to reduce these unwanted noises, which is suitable for multiple amplification. Because the error signal is a *dc* signal, which cannot be measured by the spectrum analyzer, it is only recorded by an oscilloscope. Limited by the electronic noise of the oscilloscope, we cannot read precisely the signal to noise ratio (SNR) from Figures 8 and 9. However the improvement is rather obvious by naked eye.

Last but not least, when we obtain the optimal error signal for cavity-locking by tuning the ELO phase, the error signal for phase-locking is optimized simultaneously, which does not need independent optimization. The result confirms the theoretical analysis in Section II A is correct. At the same time, it is helpful to simplify the experimental setup and adjust the process of squeezed state generation.

V. CONCLUSION

In the experiment system of squeezed state generation, limited by the weak *ac* component of the injected photodetector, it is in a dilemma between the quantum noise reduction and locking stability. In order to improve the locking performance on the premise of not affecting the squeezing degree, we design a high-gain photodetector based on the LC parallel resonant circuit. Comparing with the BPD, the gain of the RPD is about 30 dB higher at the resonant frequency. The peak-to-peak value of the error signal for cavity-locking (phase-locking) with the RPD is 240 (260) times of that with the BPD. In other words, with only 1/240 of the seed power by using the BPD, we can obtain the same locking performance with the RPD, which is benefit of reducing the classical noise of squeezed state generation. At the same time, according to the generation mechanism of error signal, we build the ELOs phase relation for the cavity- and phase-locking branches, which should have 90° out of phase. A 2-way 90° power splitter circuit is adopted, which splits the ELO into two branches with 90° out of phase, meeting the requirement for cavity- and phase-locking of squeezed state generation. Although the optimal demodulation phase difference, originating from the phase change of the detected signal with the modulation frequency, is not 90°, its influence of the phase difference on the amplitude of the error signal can be neglected. By the design, we simplify the relative phase between the detected signal and ELOs for cavity- and phase-locking from two independent steps to one.

ACKNOWLEDGMENTS

The work is supported by the National Natural Science Foundation of China (Grant Nos. 61575114 and 11504220), in part by the National Key Research and Development Program of China (Grant No. 2016YFA0301401), the Program for Sanjin Scholar of Shanxi Province and the program for Outstanding Innovative Teams of Higher Learning Institutions of Shanxi.

[1]M. B. Gray, D. A. Shaddock, C. C. Harb, and H. A. Bachor, Rev. Sci. Instrum. **69**, 3755–3762 (1998).
[2]E. D. Black, Am. J. Phys. **69**, 79 (2001).
[3]T. Eberle, V. Handchen, and R. Schnabel, Opt. Express **21**, 11546 (2013).
[4]J. I. Thorpe, K. Numata, and J. Livas, Opt. Express **16**, 15980 (2008).
[5]Y. Luo, H. Li, H. C. Yeh, and J. Luo, Rev. Sci. Instrum. **87**(5), 056105 (2016).
[6]H. Zhou, W. Yang, Z. Li, X. Li, and Y. Zheng, Rev. Sci. Instrum. **85**(1), 013111 (2014).
[7]H. Zhou, W. Wang, C. Chen, and Y. Zheng, IEEE Sens. J. **15**(4), 2101–2105 (2015).
[8]X. Jin, J. Su, Y. Zheng, C. Chen, W. Wang, and K. Peng, Opt. Express **23**(18), 23859 (2015).
[9]H. Vahlbruch, "Squeezed light for gravitational wave astronomy," Ph.D. dissertation (Gottfried Wilhelm Leibniz Universität Hannover Hannover, Germany, 2008).
[10]C. K. Alexander, M. N. Sadiku, and M. Sadiku, *Fundamentals of Electric Circuits* (McGraw-Hill Higher Education, 2007).
[11]H. Grote, Rev. Sci. Instrum. **78**, 054704 (2007).
[12]T. E. Darcie, B. L. Kaspar, and J. R. Talman, J. Lightwave Technol. **6**(4), 582–589 (1988).
[13]T. Y. Lin, R. J. Green, and P. B. O'Connor, Rev. Sci. Instrum. **82**, 124101 (2011).
[14]S. Savikhin, Rev. Sci. Instrum. **66**, 4470 (1995).
[15]H. Vahlbruch, M. Mehmet, S. Chelkowski, B. Hage, A. Franzen, N. Lastzka, S. Goer, K. Danzmann, and R. Schnabel, Phys. Rev. Lett. **100**, 033602 (2008).
[16]X. L. Su, Y. P. Zhao, S. H. Hao, X. J. Jia, C. D. Xie, and K. C. Peng, Opt. Lett. **37**, 5178 (2012).
[17]R. Senani, A. K. Singh, and V. K. Singh, *Current Feedback Operational Amplifiers and their Applications* (Springer Science and Business Media, 2013).
[18]B. Carter, *Op Amps for Everyone* (Posts and Telecom Press, 2010).
[19]E. Flaxer, Meas. Sci. Technol. **17**(8), N37 (2006).
[20]T. Lin, Y. Zhang, Y. H. Lee, H. J. Krause, and J. Lin, Rev. Sci. Instrum. **85**(11), 114708 (2014).
[21]J. C. Doyle, B. A. Francis, and A. R. Tannenbaum, *Feedback Control Theory* (Courier Corporation, 2013).
[22]Y. Luo, H. Li, H. C. Yeh, and J. Luo, Rev. Sci. Instrum. **86**(4), 044501 (2015).